EPJ manuscript No.
(will be inserted by the editor)

Hyperon production and polarization with CLAS

Sergio Anefalos Pereira[1,a]
(for the CLAS collaboration)

Instituto Nazionali di Fisica Nucleare
Laboratori Nazionali di Frascati

Abstract. Quark models with approximate SU(6) $\bigotimes$ O(3) symmetry predict more states than have been found experimentally. This is often referred to as the "missing" resonance problem. A comprehensive study of electromagnetic strangeness production has been undertaken at Jefferson Lab using the CLAS detector, circularly and linear polarized photon beams and polarized hydrogen and deuterium targets. In this paper the first measurement of the unpolarized $\gamma n(p) \rightarrow K^+\Sigma^-(p)$ differential cross section over a wide range of kaon scattering angles (from 10° to 140°) and photon energies (from 1.0 to 3.6 GeV) will be presented. Also an overview of the experiments using polarized photons and targets will be discussed.

1 Introduction

A major goal of hadron physics is to study the structure of the nucleon and its excited states. In quark models the number of excited states is determined by the effective degrees of freedom, while their ordering and decay properties are related to the residual quark-quark interaction [1]. A different class of models uses interactions that give rise to a quark-diquark clustering within the baryon [2]. More states are provided by collective models of the baryon, like the algebraic approach [3], or flux-tube models [4], which are motivated by lattice QCD. So far, however, the experimentally observed number of states is still far lower than predicted, leading to the so-called "missing resonance" problem [5].

Experimentally, most of our present knowledge of baryon resonances comes from reactions involving pions in the initial and/or final states. Photoproduction of non-strange resonances decaying into KY final states is expected to differ from those decaying into πN and $\pi\pi N$ final states [6]. Therefore, looking in the strangeness sector casts a different light on the resonance excitation spectrum, and thus, may emphasize resonances not revealed in πN scattering. To date, however, the PDG compilation [7] gives poorly-known $K\Lambda$ couplings for only five well-established resonances, and no $K\Sigma$ couplings for any resonances. Mapping out the spectrum of excited states that decay into KY particles is therefore crucial to provide a deeper insight into the underlying degrees of freedom of the nucleon and to discriminate among different models.

[a] e-mail: sergio.pereira@lnf.infn.it

In addiction to this, for Y-photoproduction on the neutron one can take full advantage of the isospin symmetry of the triplet, putting significant constraints on the γKNY coupling constants [8]. By comparing bound and free proton results, using hydrogen and deuterium targets, final state interactions can be estimated and YN interactions can be studied.

2 Jefferson Lab and the CLAS detector

The CEBAF (Continuous Electron Beam Accelerator Facility) accelerator at Jefferson Lab is capable of delivering electrons with an energy range of 0.8-6.0 GeV, a current of 200μA and and beam polarization of $\sim$ 85%. It can simultaneously deliver beams to 3 Halls. The CLAS (Cebaf Large Acceptance Spectrometer) [9] utilizes a non-uniform toroidal magnetic field generated by six superconducting coils which define six independent modules. The detector is instrumented with three sets of multi-wire drift chambers (DC) for charged track reconstruction. Two layers of scintillator counters (TOF) and lead-scintillator electromagnetic calorimeters (EC) provide charged-particle time-of-flight measurements and neutral particle measurement, respectively. The photon tagger can produce a tagged bremsstrahlung photon beam with 20-95% of the electron beam energy [10].

The targets can be longitudinally and transversely polarized with respect to the incident beam. Before 2010, the Hall-B polarized target has been used only in electron beam experiments due to the limited angular coverage in the forward direction imposed by the two 5 Tesla Helmholtz coils [11]. The FROzen Spin Target (butanol) with longitudinal and transverse polarization was designed to minimize this problem. The target material is polarized outside of CLAS and is then placed inside it. In 2010, the FROST experiment finished a successful data-taking period with polarizations of $82 - 85\%$. It demonstrated excellent reliability, running continuously for several months.

3 Physics Observables

As part of a comprehensive study of electromagnetic strangeness production at Jefferson Lab, a complete set of observables has been measured. In order to determine the transversity amplitudes in pseudoscalar meson photoproduction, without discrete ambiguities, four complex helicity amplitudes are necessary, at each energy and angle, resulting in 16 measured spin observables [12], as described in Table 1. In the channels involving hyperons, their self-analyzing weak decay presents another advantage. It allows recoil polarization measurements with high statistics, giving access to all observables. The differential cross section, $\sigma(\Theta)$, plus 3 single-spin observables, beam (Σ), target (T) and recoil polarization (P), are denoted as Type S measurements. In addition, there are 12 double-spin observables which can be classified into three types: beam-target (BT), beam-recoil (BR), and target-recoil (TR). In the next few years, all 16 spin observables will be measured for the first time.

The CLAS collaboration has already published results on $\sigma(\Theta)$, P and polarization transfer (C_x/C_z) for the reactions $\gamma p \to K^+\Lambda$ and $\gamma p \to K^+\Sigma^0$ [13–15]. New results have been published using the $g11$ unpolarized data set [16,17]. Using the $g8b$ data taken with linearly polarized photon beams, results on Σ, T, O_x and O_z will be published soon [18]. The remaining BT and TR double-spin observables have already been measured by the $FROST$ experiment [19] with longitudinal and transverse polarized targets. The last part of $FROST$ data-taking has finished in August 2010 and data-processing has begun.

Table 1. Spin observables: The 16 spin observables are classified into four types: S for the differential cross section and single-spin observables, and BT, BR, and TR for beam-target, beam-recoil, and target-recoil spin observables, respectively [12].

Spin observable	Helicity representation	Transversity representation	BHP form	Set
$\check{\Omega}^1 \equiv \check{\mathcal{I}}(\theta)$	$\frac{1}{2}(\lvert H_1\rvert^2+\lvert H_2\rvert^2+\lvert H_3\rvert^2+\lvert H_4\rvert^2)$	$\frac{1}{2}(\lvert b_1\rvert^2+\lvert b_2\rvert^2+\lvert b_3\rvert^2+\lvert b_4\rvert^2)$	$\frac{1}{2}\langle b\lvert\widetilde{\Gamma}^1\rvert b\rangle$	
$\check{\Omega}^4 \equiv \check{\Sigma}$	$\mathrm{Re}(-H_1H_4^*+H_2H_3^*)$	$\frac{1}{2}(\lvert b_1\rvert^2+\lvert b_2\rvert^2-\lvert b_3\rvert^2-\lvert b_4\rvert^2)$	$\frac{1}{2}\langle b\lvert\widetilde{\Gamma}^4\rvert b\rangle$	$\mathcal{S}$
$\check{\Omega}^{10} \equiv -\check{T}$	$\mathrm{Im}(H_1H_2^*+H_3H_4^*)$	$\frac{1}{2}(-\lvert b_1\rvert^2+\lvert b_2\rvert^2+\lvert b_3\rvert^2-\lvert b_4\rvert^2)$	$\frac{1}{2}\langle b\lvert\widetilde{\Gamma}^{10}\rvert b\rangle$	
$\check{\Omega}^{12} \equiv \check{P}$	$\mathrm{Im}(-H_1H_3^*-H_2H_4^*)$	$\frac{1}{2}(-\lvert b_1\rvert^2+\lvert b_2\rvert^2-\lvert b_3\rvert^2+\lvert b_4\rvert^2)$	$\frac{1}{2}\langle b\lvert\widetilde{\Gamma}^{12}\rvert b\rangle$	
$\check{\Omega}^3 \equiv \check{G}$	$\mathrm{Im}(H_1H_4^*-H_3H_2^*)$	$\mathrm{Im}(-b_1b_3^*-b_2b_4^*)$	$\frac{1}{2}\langle b\lvert\widetilde{\Gamma}^3\rvert b\rangle$	
$\check{\Omega}^5 \equiv \check{H}$	$\mathrm{Im}(-H_2H_4^*+H_1H_3^*)$	$\mathrm{Re}(b_1b_3^*-b_2b_4^*)$	$\frac{1}{2}\langle b\lvert\widetilde{\Gamma}^5\rvert b\rangle$	$\mathcal{BT}$
$\check{\Omega}^9 \equiv \check{E}$	$\frac{1}{2}(\lvert H_1\rvert^2-\lvert H_2\rvert^2+\lvert H_3\rvert^2-\lvert H_4\rvert^2)$	$\mathrm{Re}(b_1b_3^*+b_2b_4^*)$	$\frac{1}{2}\langle b\lvert\widetilde{\Gamma}^9\rvert b\rangle$	
$\check{\Omega}^{11} \equiv \check{F}$	$\mathrm{Re}(-H_2H_1^*-H_4H_3^*)$	$\mathrm{Im}(b_1b_3^*-b_2b_4^*)$	$\frac{1}{2}\langle b\lvert\widetilde{\Gamma}^{11}\rvert b\rangle$	
$\check{\Omega}^{14} \equiv \check{O}_x$	$\mathrm{Im}(-H_2H_1^*+H_4H_3^*)$	$\mathrm{Re}(-b_1b_4^*+b_2b_3^*)$	$\frac{1}{2}\langle b\lvert\widetilde{\Gamma}^{14}\rvert b\rangle$	
$\check{\Omega}^7 \equiv -\check{O}_z$	$\mathrm{Im}(H_1H_4^*-H_2H_3^*)$	$\mathrm{Im}(-b_1b_4^*-b_2b_3^*)$	$\frac{1}{2}\langle b\lvert\widetilde{\Gamma}^7\rvert b\rangle$	$\mathcal{BR}$
$\check{\Omega}^{16} \equiv -\check{C}_x$	$\mathrm{Re}(H_2H_4^*+H_1H_3^*)$	$\mathrm{Im}(b_1b_4^*-b_2b_3^*)$	$\frac{1}{2}\langle b\lvert\widetilde{\Gamma}^{16}\rvert b\rangle$	
$\check{\Omega}^2 \equiv -\check{C}_z$	$\frac{1}{2}(\lvert H_1\rvert^2+\lvert H_2\rvert^2-\lvert H_3\rvert^2-\lvert H_4\rvert^2)$	$\mathrm{Re}(b_1b_4^*+b_2b_3^*)$	$\frac{1}{2}\langle b\lvert\widetilde{\Gamma}^2\rvert b\rangle$	
$\check{\Omega}^6 \equiv -\check{T}_x$	$\mathrm{Re}(-H_1H_4^*-H_2H_3^*)$	$\mathrm{Re}(-b_1b_2^*+b_3b_4^*)$	$\frac{1}{2}\langle b\lvert\widetilde{\Gamma}^6\rvert b\rangle$	
$\check{\Omega}^{13} \equiv -\check{T}_z$	$\mathrm{Re}(-H_1H_2^*+H_4H_3^*)$	$\mathrm{Im}(b_1b_2^*-b_3b_4^*)$	$\frac{1}{2}\langle b\lvert\widetilde{\Gamma}^{13}\rvert b\rangle$	$\mathcal{TR}$
$\check{\Omega}^8 \equiv \check{L}_x$	$\mathrm{Re}(H_2H_4^*-H_1H_3^*)$	$\mathrm{Im}(-b_1b_2^*-b_3b_4^*)$	$\frac{1}{2}\langle b\lvert\widetilde{\Gamma}^8\rvert b\rangle$	
$\check{\Omega}^{15} \equiv \check{L}_z$	$\frac{1}{2}(-\lvert H_1\rvert^2+\lvert H_2\rvert^2+\lvert H_3\rvert^2-\lvert H_4\rvert^2)$	$\mathrm{Re}(-b_1b_2^*-b_3b_4^*)$	$\frac{1}{2}\langle b\lvert\widetilde{\Gamma}^{15}\rvert b\rangle$	

Concerning deuterium targets, Jefferson Lab has performed two experiments named $g10$ (unpolarized) and $g13$ (with circularly and linearly polarized beams). The first measured the $\gamma n \to K^+\Sigma^-$ cross sections and the second has several KY analyses ongoing.

4 Photoproduction on protons

4.1 Unpolarized cross section

When CLAS published the $\gamma p \to K^+\Lambda$ cross sections [13], a clear disagreement with previous data from SAPHIR [20] was evident. This difference was the subject of various debates, and a third measurement was needed to settle the discussion. A new measurement was done using the $g11$ data set. The new data have a broader energy range, from threshold up to 2.84 GeV, with improved statistics. The comparison with the previous published data for one bin of $0.35 \leq cos\Theta \leq 0.45$ of the kaon in the KY center-of-mass frame is shown in the left plot of Figure 1. The latest analysis was done with a different data set, different trigger and different analysis chain, confirming the earlier CLAS results. The agreement between previous CLAS [13] and new CLAS data sets [16] is excellent. Also shown in Figure 1 (right plot) is the $\gamma p \to K^+\Sigma^0$ cross section [17] from the same data set and the same angular bin, compared with the previous CLAS [13] and SAPHIR results [20]. Overall, the agreement among the three data sets is very good.

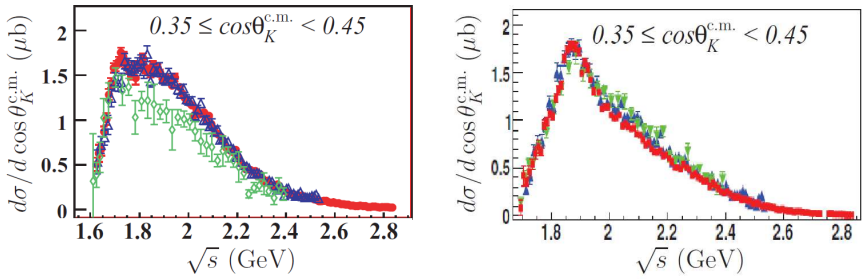

Fig. 1. (Color online) Differential cross sections $\gamma p \to K^+\Lambda$ (left plot) and $\gamma p \to K^+\Sigma$ (right plot) for the angular bin $0.35 \leq cos\Theta \leq 0.45$ of the kaon in the KY center-of-mass frame. The new CLAS data (red points) are compared with previous CLAS results (blue markers) [13] and SAPHIR (green markers) [20].

Using a coupled-channels approach [21] the previous CLAS data [13] were reproduced reasonably well adding the $S_{11}(1806)$, $P_{13}(1893)$ and $D_{13}(1954)$ resonances, as can be seen in Figure 2, for three different bins of $cos\Theta$ of the kaon in the KY center-of-mass frame. Alternative approaches propose other contributions for the resonance-like structure at 1.9 GeV like D_{13} [22], P_{13} [23,24], P_{11} [25] and also a $\bar{K}KN$ bound state [26], which is a newly predicted bound state with a mixture of $a_0(980)N$ and $f_0(980)N$.

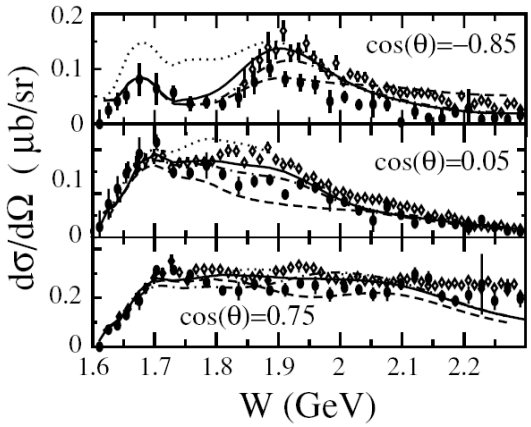

Fig. 2. Differential cross sections for the reaction $\gamma p \to K^+\Lambda$ as a function of total-center-of-mass energy for three different bins of $cos\Theta$ of the kaon in the KY center-of-mass frame. The solid curve corresponds to the full model. Dotted, dot-dashed, and dashed curves correspond to the full model without the third S_{11}, third P_{13} and third D_{13} resonances, respectively. Data are from CLAS [13] (open diamonds) and SAPHIR [20] (full circles).

4.2 Single beam polarization

The experiment *g8b* measured the $K^+\Lambda$ linearly polarized photon asymmetry (Σ). These new results have a wider range, $E_\gamma = 1.1 - 2.2$ GeV and $-0.75 \leq cos(\Theta)_K^{CM} \leq$

0.85, and higher precision in comparison with the available published data, and are in good agreement with GRAAL [27] and LEPS [28] data, as can be seen in the left plot of Figure 3 ($E_\gamma = 1.55$ GeV). Also, in the right plot ($E_\gamma = 1.175$ GeV) one can see that the angular coverage at backward angles was increased significantly.

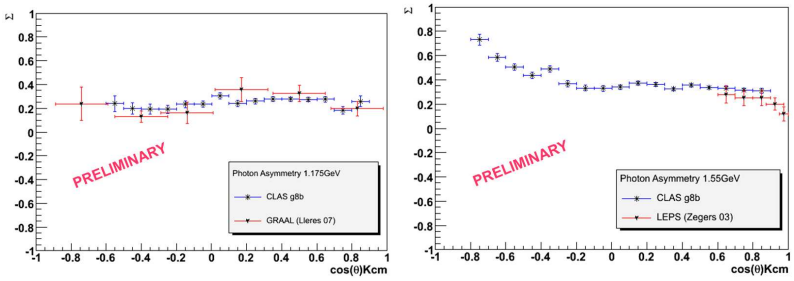

Fig. 3. (Color online) Photon beam asymmetries for the $\gamma p \to K^+\Lambda$ channel as a function of $cos(\Theta)$ of the kaon in the KY center-of-mass frame for the photon energy bin $E_\gamma = 1.175$ GeV (left) and $E_\gamma = 1.55$ GeV (right). The CLAS data (blue bars) are compared to GRAAL [27] and LEPS [28], respectively.

4.3 Recoil polarization

The same $g11$ data set also provided new measurements of the hyperon recoil polarization (P) for the $\gamma p \to K^+\Lambda$ [16] and $\gamma p \to K^+\Sigma$ [17] reactions. These new results cover a wider W range, from threshold up to 2.84 GeV, with better precision, as can be seen in Figure 4. With the new results, a more detailed structure is now visible. For the Λ channel the agreement among the new CLAS results [16], previous CLAS [14] results, SAPHIR [20] and GRAAL [27] are very good. For the Σ channel, the new CLAS [17] results are compared with the previous CLAS [14] data.

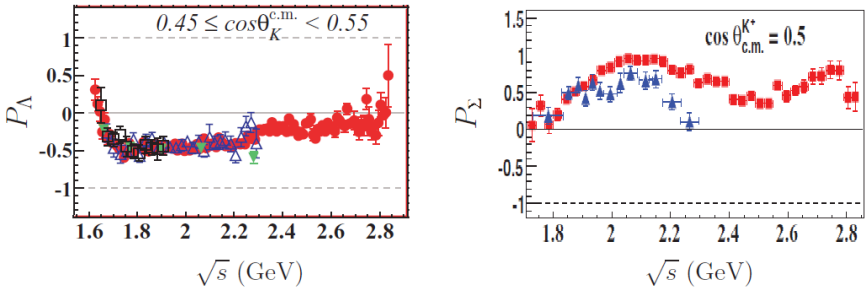

Fig. 4. (Color online) Λ recoil polarization for the $\gamma p \to K^+\Lambda$ channel (left plot) and Σ recoil polarization for the $\gamma p \to K^+\Sigma$ channel (right plot) in the angular bin of $0.45 \leq cos\Theta \leq 0.55$ of the kaon in the KY center-of-mass frame. For the Λ channel, the new CLAS results are represented by red circles [16], previous CLAS results by blue triangles, SAPHIR [20] by green triangles, and GRAAL [27] by black squares. For the Σ channel, the new CLAS results (red squares) [17] are compared with earlier CLAS [14] results (blue triangles).

4.4 Double polarization (BR) with a circularly polarized beam

Polarization transfer variables (C_x and C_z) obtained with CLAS [15], covering $W = 1.6 - 2.53$ GeV and $-0.85 \leq cos(\Theta)_K^{CM} \leq 0.95$, have provided very important data to constrain theoretic models. Theoretical predictions have poorly reproduced these observables. Using CLAS results the fit was redone with the Bonn-Gachina multi-coupled-channel isobar model, including several resonances such as S_{11}-wave, $P_{13}(1720)$, $P_{13}(1900)$ and $P_{11}(1840)$ [24]. The predictive power of the models has improved significantly with the inclusion of $P_{13}(1900)$, but not with $P_{11}(1900)$ or $D_{13}(1900)$, as can be seen in Figure 5. Also, $K^+\Sigma^0$ cross sections (not shown) are better described with $P_{13}(1900)$. These results suggest that this resonance could be promoted from ** to **** status. It is very important to point out that this $P_{13}(1900)$ resonance is not found in quark-diquark models [29] .

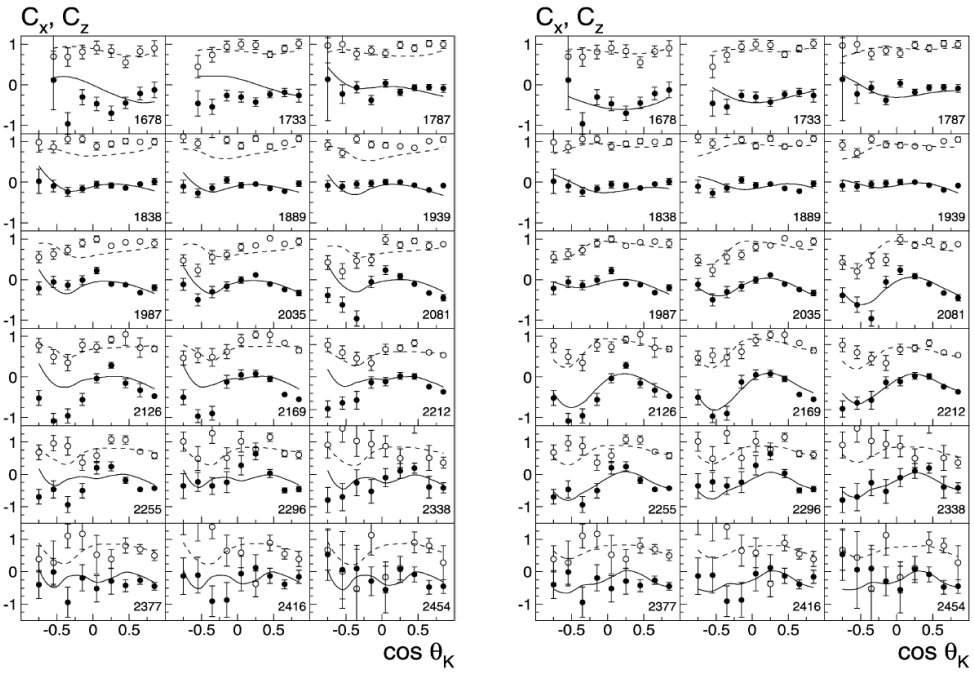

Fig. 5. Comparison between the Λ polarization transfer predictions with (right distributions) and without (left distributions) the $P_{13}(1900)$ resonance. Open circles are C_z and full circles C_x.

Another important recent CLAS result is the total Λ polarization [15]. The quadratic sum of all polarization components $R^2 \equiv P^2 + C_x^2 + C_z^2$, which has a maximum of 1, is consistent with +1 across all values of W and kaon angles, as can be seen in Figure 6. The weighted mean over the data at all energies and angles gives $R_\Lambda = 1.01 \pm 0.01$, which is highly unexpected. In the case of the $K^+\Sigma^0$ channel the total Σ^0 polarization was found to be $R_\Sigma = 0.82 \pm 0.03$, which is definitely different from +1. The reason why the Λ is formed fully spin-polarized but not the Σ^0 is still unknown.

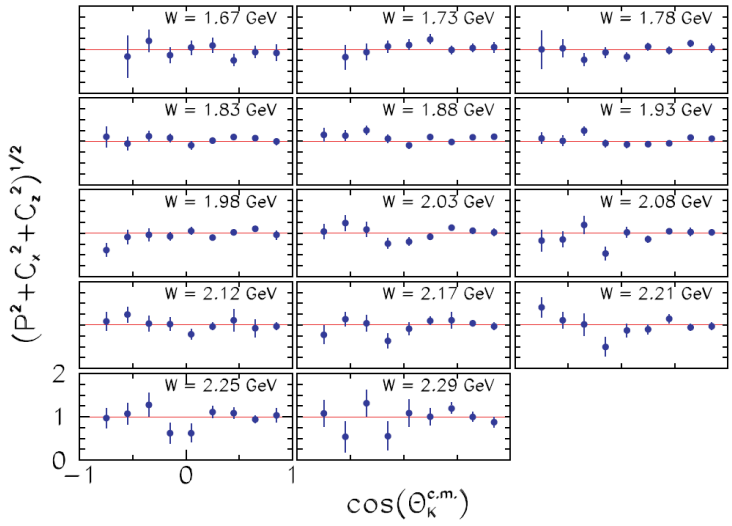

Fig. 6. (Color online) Magnitude of the hyperon polarization observable $R_\Lambda = P^2+C_x^2+C_z^2$ versus $cos(\Theta)$ of the kaon in the KY center-of-mass frame. Lower-left axis scales apply to all plots. R is consistent with unity over all values of W and kaon angles.

5 Photoproduction on neutrons

5.1 Unpolarized cross section

Cross section data of hyperon photoproduction on neutrons are very scarce. Recently, CLAS has measured the $\gamma d \to \Sigma^- K^+(p)$ differential cross section [30]. The differential cross sections for fixed photon energy as a function of $cos(\Theta)$ of the kaon in the KY center-of-mass frame are shown in Figure 7. The error bars represent the total error (statistical plus systematic). At a photon energy of ~ 1.8 GeV, a clear forward peak starts to appear and becomes more prominent as the photon energy increases. This behavior, which is typically attributed to contributions from t-channel mechanisms, is not observed at lower energies, where the dominant contributions appear to be from s-channel mechanisms. Above $\sim$2.1 GeV there are indications of a possible backward peak, which might suggest the presence of u-channel mechanisms.

The few LEPS data [31] available for energies 1.5–2.4 GeV and at forward angles are also shown in Fig. 7. They are in good agreement with our results within the total uncertainties.

Also shown in Fig. 7 are the theoretical results of a Regge-based calculation (Regge-3 model) [32]. In this model, the reaction amplitude incorporates the exchange of K^+ and $K^*(892)^+$ Regge trajectories. By adding resonance contributions to the Regge amplitudes, the model is able to describe the Λ and Σ^0 photo- and electro-production data on the proton reasonably well. The Regge-based model overestimates our results at forward and intermediate angles by about a factor of two. At backward angles the calculated cross section is too small by an order or magnitude, which is a reflection of the lack of resonances in the model.

New neutron data will be available soon from the $g13$ experiment with circularly and linearly photon beams and a deuterium target.

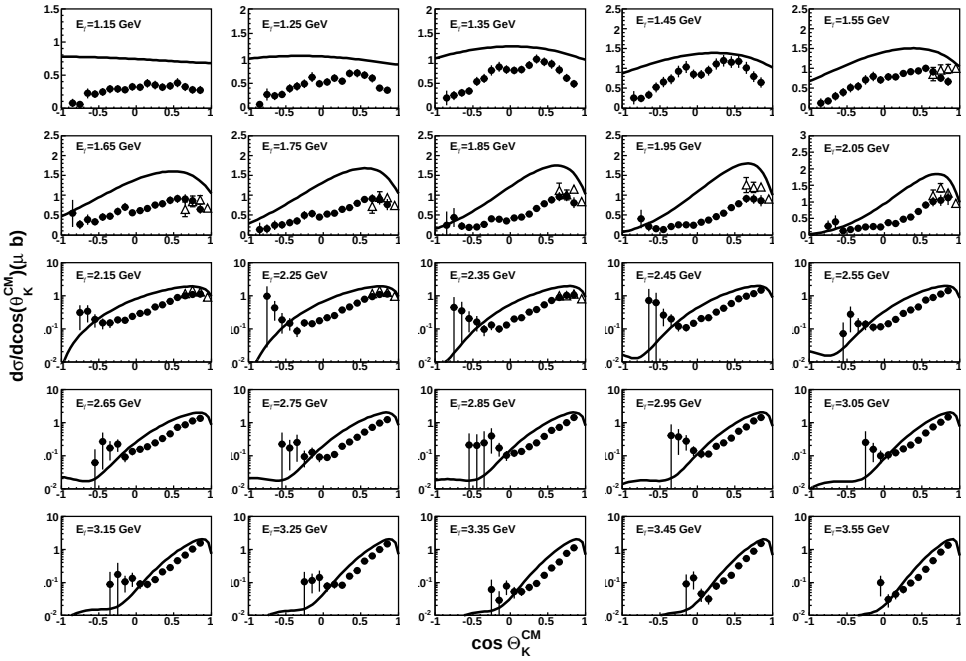

Fig. 7. Differential cross sections for the reaction $\gamma n(p) \to K^+\Sigma^-(p)$ obtained by CLAS [30] (black circles). The error bars represent the total (statistical plus systematic) uncertainty. Data from LEPS [31] (empty triangles) and Regge-3 model prediction [32] (solid curve) are also shown.

6 Conclusions

The CLAS detector at CEBAF provides very precise measurements in a broad kinematic range in KY photoproduction, offering kinematic and analysis advantages in N* physics. Published CLAS KY results on the proton (Σ, P, C_x, C_z) have favored a $P_{13}(1900)$ (not $P_{11}(1900)$ or $D_{13}(1900)$) resonance. More single-spin observables (Σ, P) and new beam-recoil (O_x, O_z) observables will be published soon. The remaining beam-target (G, E) and target-recoil (L_x, L_z) results are in the analysis pipeline of FROST. Cross sections for the $\gamma n \to K^+\Sigma^-$ channel over a wide photon energy and angular range have been obtained with CLAS during the $g10$ experiment for the first time, and more results with polarized photon beams are coming in the next couple of years.

References

1. S. Capstick and W. Roberts, Prog. Part. Nucl. Phys. **45**, 241 (2000); A. J. G. Hey and R. L. Kelly, Phys. Reports **96**, 71 (1983).
2. M. Anselmino *et al.*, Rev. Mod. Phys. **65**, 1199 (1993).
3. R. Bijker *et al.*, Ann. of Phys. **236**, 69 (1994).
4. N. Isgur and J. Paton, Phys. Rev. D **31**, 2910 (1985).
5. N. Isgur and G. Karl, Phys. Rev. D **18**, 4187 (1978); Phys. Rev. D **19**, 2653 (1979) and Phys. Rev. D **20**, 1191 (1979).

6. S. Capstick and W. Roberts, Phys. Rev. D **49**, 4570 (1994); Phys. Rev. D **57**, 4301 (1998) and Phys. Rev. D **58**, 74011 (1998).
7. C. Amsler *et al.* (Particle Data Group), Phys. Lett. B **667**, 1 (2008).
8. T. Mart, C. Bennhold and C.E.Hyde-Wright, Phys. Rev. C **51**, 1074(R) (1995).
9. B. A. Mecking *et al.*, Nucl. Instrum. Methods A **503**, 444 (2003).
10. D. I. Sober *et al.*, Nucl. Instrum. Methods A **440**, 263 (2000).
11. C. D. Keith *et al.*, Nucl. Instrum. Methods A **501**, 327 (2003).
12. Wen-Tai Chiang and Frank Tabakin, Phys. Rev. C **55**, 2054 (1997).
13. R. Bradford *et al.*, Phys. Rev. C **73** 035202 (2006).
14. J. McNabb *et al.*, Phys. Rev. C **69** 042201 (2004).
15. R. Bradford *et al.* Phys. Rev. C **75** 035205 (2007).
16. M.E. McCracken *et al.* Phys. Rev. C **81** 025201 (2010).
17. B. Dey *et al.* Phys. Rev. C **82** 025202 (2010).
18. C. Paterson, Ph.D. thesis 2008, University of Glasgow web: http://www.jlab.org/Hall-B/general/clas_thesis.html, and to be published.
19. E. Pasyuk *et al.*, arXiv:0906.4221v1[hep-ex].
20. K. -H. Glander *et al.*, Eur. Phys. J. A **19**, 251 (2004).
21. B. Julia-Diaz *et al.*, Phys. Rev. C **73**, 055204 (2006).
22. T. Mart and C. Bennhold, Phys. Rev. C **61**, 012201(R) (1999).
23. A. V. Sarantsev *et al.*, Eur. Phys. J. A **25**, 441 (2005); A. Anisovich *et al.*, Eur. Phys. J. A **24**, 111 (2005); A. V. Anisovich, *et al.*, Eur. Phys. J. A **25**, 427 (2005).
24. V. A. Nikonov *et al.*, Phys. Lett. B **662**, 245 (2008) [arXiv:0707.3600 [hep-ph]].
25. M. Guidal, J.-M. Laget, and M. Vanderhaeghen, Nucl. Phys. **A627**, 645 (1997); M. Guidal, J.-M. Laget, and M. Vanderhaeghen, Phys. Rev. C **61**, 025204 (2000).
26. A. Martinez Torres *et al.*, Eur. Phys. J. A **41**, 361 (2009) [arXiv:0902.3633 [nucl-th]].
27. A. Lleres *et al.*, Eur. Phys. J. A **31**, 79 (2007).
28. R. G. T. Zegers, M. Sumihama *et al.*, Phys. Rev. Lett. **91** 092001 (2003).
29. E. Santopinto, Phys Rev. C **72**, 022201 (2005).
30. S. Anefalos Pereira *et al.*, Phys. Lett. B **688** 289 (2010).
31. H. Kohri *et al.*, Phys. Rev. Lett. **97**, 082003 (2006).
32. P. Vancraeyveld, L. De Cruz, J. Ryckebusch, T. Van Cauteren, Phys. Lett. B **681** 428 (2009).